

OFFICIAL JOURNAL OF THE BRITISH HOROLOGICAL INSTITUTE

The Horological Journal



JULY 2024
www.bhi.co.uk



An Improved Calendar Ring Hole-Count for the Antikythera Mechanism

A Fresh Analysis



Graham Woan



Joseph Bayley

Abstract

We present a new analysis of the positions of holes beneath the calendar ring of the Antikythera Mechanism, as measured by Budiselic *et al.* (2020). We significantly refine their estimate for the number of holes that were present in the full ring. Our 68%-credible estimate for this number, taking account of all the data, is $355.24^{+1.39}_{-1.36}$. If holes adjacent to fractures are removed from the analysis, our estimate becomes $354.08^{+1.47}_{-1.41}$. A ring of 360 holes is strongly disfavoured, and one of 365 holes is not plausible, given our model assumptions.

1. Introduction

The Antikythera Mechanism is a multi-component device recovered from a shipwreck close to the Greek island of Antikythera in 1901. It is believed to be the remains of a complex mechanical calculator of ancient origin, and has undergone considerable investigation and analysis to determine its true form and function³.

In a recent paper¹, Budiselic *et al.* presented new, high resolution X-ray data on one of the components of the mechanism – the so-called front dial calendar ring – found in fragment C. Only a part of the full ring survives, and it is fractured into several sections.

Budiselic *et al.* made careful measurements of the positions of closely spaced holes beneath the ring. These holes are thought to have been used to rotationally align the calendar ring, and their number is crucial for the interpretation of the ring's function. The authors generously made their measurements of the hole positions available⁵, and this paper is based entirely on these data.

In this paper, we infer the number of holes that were present in the complete ring, \mathcal{N} , given these measurements and some reasonable assumptions. Budiselic *et al.* presented an analysis that resulted in an estimator for \mathcal{N} with a 99% confidence interval of 346.8 to 367.2. However, using the same data, a clearer and more stringent statement can be made about \mathcal{N} using a Bayesian analysis and an improved model for the positional errors in hole placement.

Bayesian methods have several distinct advantages over frequentist methods for addressing problems such as this: first, one can make simple probabilistic statements about the value of \mathcal{N} itself, something that frequentist methods are not able

to do, by definition. As a result, there is no need to choose a statistic of the data against which to test a null hypothesis. It is also straightforward to include all the parameters of the system in the analysis, accounting for the unknown relative orientations of the ring sections. This allows us to make a concrete statement about \mathcal{N} that is constrained by all the pertinent information in the data.

2. The Model

We assume that originally there were \mathcal{N} holes, arranged around a circle of radius r . Today, the circle is partial and fragmented, and exists as a set of s contiguous arc sections that are slightly displaced and rotated with respect to each other.

X-ray images⁵ provide data $\mathbf{d}_i = (x_i, y_i)$, $1 \leq i \leq n$, on the Cartesian co-ordinates of $n = 81$ contiguous and reportedly coplanar points (the hole centres) that sit on the arcs. Budiselic *et al.* number these, and we will use their numbering convention for both the holes and sections. The circle-centres of the section arcs are at s closely bunched, but unknown, locations $\mathbf{r}_j = (x_{0j}, y_{0j})$, $0 \leq j \leq (s-1)$ and the relative rotations of the sections are also not known precisely.

For the j th section, we take α_j as the angular position of the first hole of the full circle, when the section (in its current location and orientation) is extended to that point. Again, the sections only show minimal relative rotation, so we expect these α_j values to be very similar. The apparent angular position of the i th hole in the j th section with respect to its arc-centre is therefore

$$\phi_{ij} = 2\pi \frac{(i-1)}{\mathcal{N}} + \alpha_j. \quad (1)$$

There are, therefore, three unknown parameters for each section, $(x_{0j}, y_{0j}, \alpha_j)$, defining a displacement and a rotation in the (x, y) plane. For the moment, we will assume there are no internal distortions of the sections and that they do indeed lie in the (x, y) plane defined by the dataset.

Our goal is to determine the number of holes in the full ring, \mathcal{N} . We will use a Bayesian analysis, in which parameters such as r have an associated probability distribution function (PDF) $p(r)$, representing our degree of belief that the parameter lies within any particular range of values, defined as

$$\text{Prob}(r_1 \leq r \leq r_2) = \int_{r_1}^{r_2} p(r) dr. \quad (2)$$

Our model for the fragments will depend on a multidimensional parameter vector, \mathbf{a} , for which \mathcal{N} is just one component. Defining $\mathbf{a} = (\mathcal{N}, r, \{(x_{0j}, y_{0j})\}, \{\alpha_j\}, C)$, the PDF for \mathcal{N} alone, given the dataset $\{\mathbf{d}_i\}$, can be computed by marginalising over the other (‘nuisance’) parameters of the joint PDF, i.e.,

$$p(\mathcal{N} | \{\mathbf{d}_i\}) = \int_{\mathbf{a} \sim \mathcal{N}} p(\mathbf{a} | \{\mathbf{d}_i\}) d\mathbf{a} \propto \int_{\mathbf{a} \sim \mathcal{N}} p(\mathbf{a}) p(\{\mathbf{d}_i\} | \mathbf{a}) d\mathbf{a}, \quad (3)$$

where the integrals are over all the \mathbf{a} components except \mathcal{N} , and C represents a parameterised characterisation of random positional errors. Here, we have used Bayes’ theorem,

$$p(\mathbf{a} | \{\mathbf{d}_i\}) = \frac{p(\mathbf{a}) p(\{\mathbf{d}_i\} | \mathbf{a})}{p(\{\mathbf{d}_i\})}, \quad (4)$$

recognising that the denominator $p(\{\mathbf{d}_i\})$ (usually called the ‘evidence’) does not depend on \mathbf{a} . The $p(\mathbf{a} | \{\mathbf{d}_i\})$ term is usually called the ‘posterior probability’, $p(\mathbf{a})$ the ‘prior probability’ and $p(\{\mathbf{d}_i\} | \mathbf{a})$ the ‘likelihood’ of the parameters. Given the relatively tight tolerances in the calendar ring, we will take uniform prior probabilities for \mathcal{N} , r , $\{(x_{0j}, y_{0j})\}$ and $\{\alpha_j\}$. We will also initially regard \mathcal{N} as a continuous (rather than discrete) parameter, allowing the possibility that the hole spacing had a single discontinuity at a start/end point.

Finally, we will take a Gaussian PDF for the errors in measurement and placement of the holes. If the intended i th hole position in section j , relative to its arc centre, is \mathbf{r}_{ij} , we have an error vector

$$\mathbf{e}_{ij} = \mathbf{r}_{ij} - (\mathbf{d}_i - \mathbf{r}_{0j}), \quad (5)$$

displacing the hole from its intended position. It is likely that the ring of holes started as a precisely scribed circle. It is therefore appropriate to differentiate between errors in the radial locations of the holes, and errors around the ring, which we will regard as tangential position errors, and take these as independent. If we define $\hat{\mathbf{r}}_i$ and $\hat{\mathbf{t}}_i$ as orthogonal unit vectors aligned with these directions at the intended hole position, the noise covariance matrix in this (locally rotated) coordinate system is simply

$$C = \begin{pmatrix} \sigma_r^2 & 0 \\ 0 & \sigma_t^2 \end{pmatrix}, \quad (6)$$

where σ_r and σ_t are the (unknown) radial and tangential standard deviations. We can further assume that $\sigma_{r,t}$ are the same for every hole and that the hole-to-hole errors are uncorrelated. In these circumstances the likelihood of the parameters is

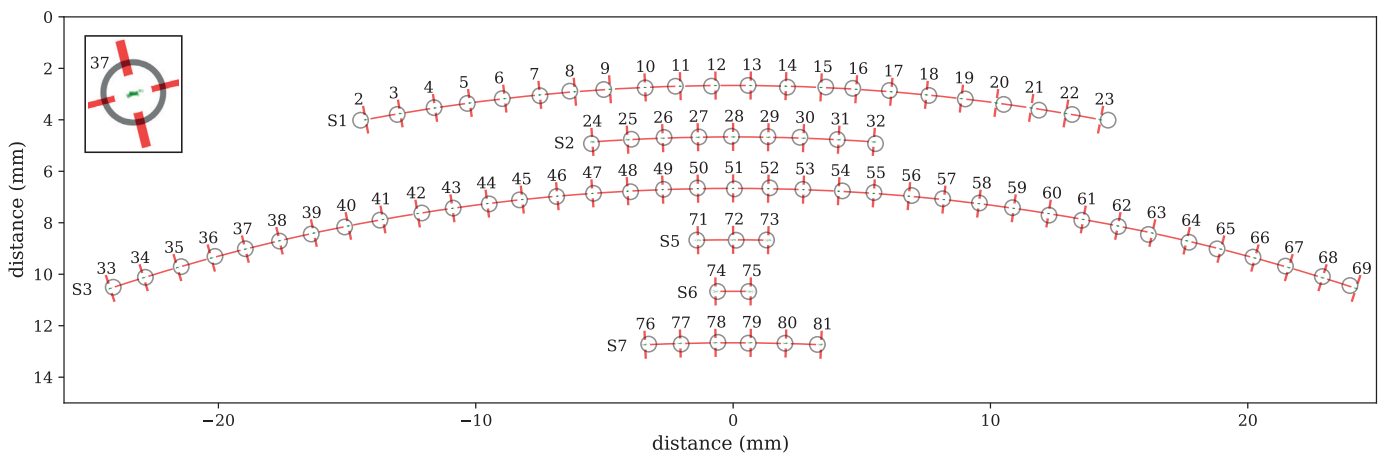
$$p(\{\mathbf{d}_i\} | \mathbf{a}) = (2\pi\sigma_r\sigma_t)^{-n} \prod_{j=0}^{s-1} \prod_i^{i \text{ in } j} \exp \left[-\frac{(\mathbf{e}_{ij} \cdot \hat{\mathbf{r}}_{ij})^2}{2\sigma_r^2} - \frac{(\mathbf{e}_{ij} \cdot \hat{\mathbf{t}}_{ij})^2}{2\sigma_t^2} \right], \quad (7)$$

where the second product is over the hole indices in the j th section, and

$$\hat{\mathbf{r}}_{ij} = (\cos \phi_{ij}, \sin \phi_{ij}), \quad (8)$$

$$\hat{\mathbf{t}}_{ij} = (\sin \phi_{ij}, -\cos \phi_{ij}). \quad (9)$$

As we will see, the errors are tiny in comparison to the radius of the ring, so there is no practical difference between errors referenced to a local tangent and errors along the circular curve. We will assume non-informative Jeffreys priors on the noise scale parameters σ_r and σ_t , (each $\propto 1/\sigma$), though in practice uniform priors on these parameters deliver almost identical results.



3. Data Analysis and Results

The ring fragment is divided into eight sections numbered 0 to 7¹ (Figure 1), each distinct and with unknown relative translations and rotations. Sections 0 and 4 each contain only one hole. These sections do not constrain any of our parameters and have therefore been omitted from the analysis. The remaining six useful sections containing a total of 79 holes, each with (x, y) co-ordinate data, supplied in millimetres, as

Figure 1. The measured (grey circles) and modelled (cross-hairs) positions of the holes in the calendar ring, broken down by section and using the median marginal values for the model parameters. The sections are aligned and stacked for ease of viewing. Fifty randomly drawn posterior predictive values of each hole position are shown in green, with hole 37 magnified to show these values more clearly. Note that \mathcal{N} is not constrained to be an integer here.

constraints. We have three parameters per section, six usable sections and four further parameters (N , r , σ_r and σ_t), making a total of 22 unknown quantities constrained by the data, and a 22-dimensional posterior space to explore.

We implemented the above analysis using two independently written codes. The first used the affine-invariant Markov Chain Monte Carlo (MCMC) ensemble sampler emcee², which provides stochastic samples drawn from the joint posterior PDF of the parameters. These samples provide estimates for both the full posterior and the parameter marginals, which are the PDFs of parameters individually, taking properly weighted account of the possible values of the other parameters.

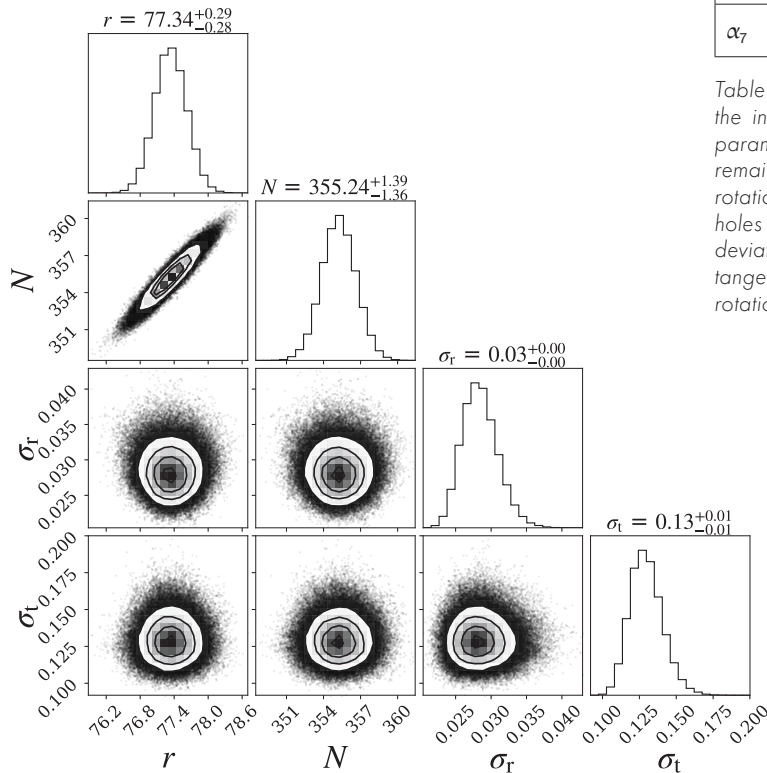
The second code used the same model, but explored the posterior space using the dynesty nested sampling algorithm⁴ and considered N as a discrete parameter as well as continuous.

We ran emcee with 100 walkers for 35 000 samples, with the first 15 000 samples discarded as burn-in. The final chains were thinned by a factor of ten before further processing and plotting. We ran dynesty with 2 000 live points, stopping when the remaining evidence was less than 1% ($\Delta \ln \mathcal{Z}_i < 0.01$) at iteration i . We will consider the dynesty results later.

3.1 Full Parameter Space Results

Table 1 shows the full set of calendar ring parameter values derived from the MCMC analysis. The results quote the medians of their marginal posteriors, and the 68%, 90%, 95% and 99% equal-tailed credible intervals.

The full posterior sits in a 22-dimensional space, and it is conventional to present it as a plot of one and two-dimensional marginal projections. Even this summary plot is too detailed for display, so in **Figure 2** we show just the plot for the intrinsic parameters N , r , σ_r and σ_t . The nested sampling code delivered results that were fully consistent with these MCMC results.



Parameter	Median	68%	90%	95%	99%
r	77.34	+0.29 -0.28	+0.47 -0.46	+0.56 -0.56	+0.75 -0.74
N	355.24	+1.39 -1.36	+2.30 -2.27	+2.75 -2.73	+3.62 -3.62
σ_r	0.028	+0.003 -0.002	+0.005 -0.004	+0.006 -0.004	+0.008 -0.005
σ_t	0.129	+0.012 -0.010	+0.020 -0.016	+0.025 -0.019	+0.035 -0.024
x_{01}	79.69	+0.20 -0.20	+0.33 -0.33	+0.40 -0.40	+0.53 -0.53
x_{02}	79.91	+0.23 -0.22	+0.38 -0.37	+0.46 -0.45	+0.61 -0.59
x_{03}	79.86	+0.03 -0.03	+0.06 -0.06	+0.07 -0.07	+0.09 -0.09
x_{05}	81.44	+1.10 -1.11	+1.84 -1.84	+2.21 -2.21	+2.91 -2.94
x_{06}	81.56	+2.46 -2.41	+4.12 -3.92	+4.91 -4.65	+6.51 -5.96
x_{07}	83.22	+0.39 -0.38	+0.64 -0.63	+0.76 -0.75	+1.01 -0.99
y_{01}	136.03	+0.21 -0.20	+0.35 -0.34	+0.41 -0.41	+0.55 -0.54
y_{02}	135.71	+0.27 -0.27	+0.45 -0.44	+0.53 -0.53	+0.70 -0.71
y_{03}	135.71	+0.29 -0.28	+0.48 -0.47	+0.57 -0.56	+0.76 -0.75
y_{05}	136.10	+0.40 -0.42	+0.66 -0.69	+0.79 -0.83	+1.05 -1.10
y_{06}	135.85	+0.80 -0.86	+1.29 -1.46	+1.51 -1.74	+1.95 -2.30
y_{07}	136.42	+0.29 -0.30	+0.49 -0.50	+0.59 -0.59	+0.78 -0.80
α_1	-145.72	+0.06 -0.06	+0.10 -0.10	+0.12 -0.12	+0.16 -0.16
α_2	-145.67	+0.19 -0.19	+0.31 -0.31	+0.37 -0.37	+0.49 -0.50
α_3	-145.54	+0.20 -0.20	+0.33 -0.33	+0.39 -0.39	+0.52 -0.53
α_5	-146.71	+0.90 -0.88	+1.50 -1.48	+1.81 -1.77	+2.38 -2.36
α_6	-146.36	+1.92 -1.93	+3.12 -3.25	+3.71 -3.86	+4.81 -5.06
α_7	-147.80	+0.42 -0.43	+0.70 -0.71	+0.83 -0.85	+1.10 -1.12

Table 1. The full marginal posterior medians and credible intervals for the inferred parameter values in the ring model. Note that only four parameters, N , r , σ_r and σ_t , are intrinsic to the calendar ring. The remaining 18 (extrinsic) parameters define the coplanar translational and rotational positions of the six fragments considered. N is the number of holes in the full ring, r the radius of the full ring, and σ_r and σ_t the standard deviations of the holes from their intended positions in the radial and tangential directions. $(x_{0i}, y_{0i}, \alpha_i)$ are the locations (in millimetres) and rotation angles (in degrees) of the ring sections.

Figure 2. Posterior corner plot for the intrinsic (N , r , σ_r and σ_t) parameters of the calendar ring, based on all sections except 0 and 4, and marginalised over the other 18 extrinsic parameters. Length units are millimetres. The expected positive correlation between r and N is clear in their joint marginal plot.

Figure 1 shows the hole position data (grey circles) and the median parameter solutions for the hole positions (red cross-hairs and arcs). The figure also contains 50 posterior predictive values for each hole position. These positions are computed from representative parameter values drawn from their joint posterior PDF, and will therefore be highly correlated. The positions of these relative to the actual hole positions highlight the relative magnitude of the radial and tangential errors. Most of the positional error is tangential, which justifies the use of an anisotropic covariance matrix.

3.2 Discussion of the Full Parameter Space Results

We performed several additional runs using only subsets of the ring sections. Unsurprisingly, most of the information on \mathcal{N} and r resides in sections 1, 2 and 3. The other sections are not long enough to constrain r well and, as a result, they have relatively little impact on the derived value of \mathcal{N} . In principle, it is harmless to include these relatively uninformative sections in the analysis, but there is a danger these smaller sections, and the extremities of the larger sections, contain outliers that are not consistent with our assumptions. We will consider this in Section 3.4.

The results in **Table 1** show that the radial error in the hole positions is less than a quarter of the tangential error. It appears that the manufacturer did a better job at putting points on a circle than spacing them evenly, and this insight has a direct bearing on the precision with which we can estimate r , and therefore \mathcal{N} .

Our noise model allows for a tighter constraint on r than would be possible with an analysis that does not take this asymmetry into account. Indeed, an analysis that does not make this distinction returns an uncertainty in the value of \mathcal{N} that is approximately three times higher.

One might imagine that the manufacture began with a circle scribed in the metal, using a pair of dividers, and that the holes were marked around this circle with a punch. If the punch was seated in the scribed groove, the radial error would indeed be very small and largely dependent on the angle at which the punch was struck. In contrast, each azimuthal position of the punch requires a separate measurement, and would suffer a larger hole-to-hole variation.

However, we note that the degree of manufacturing precision is remarkable, with standard errors in hole positions of only 0.028 mm radially, and 0.129 mm azimuthally. Budiselic *et al.* quote a standard deviation for their individual position measurements of 0.037 mm, so a good deal of the radial error may come from the measurements of the X-ray images themselves.

Taking \mathcal{N} as a continuous parameter, and with our other assumptions on the noise statistics, our 99% credible interval for the number of holes in the full circle is $355.24^{+3.62}_{-3.62}$. The same interval for the radius of the ring is $77.34^{+0.75}_{-0.74}$ mm. This appears to compare favourably with the results of Budiselic *et al.*, with the proviso that their confidence intervals are not to be interpreted as intervals that contain the true value with the specified confidence. Only Bayesian statements can be phrased in that way and, given our assumptions, we are 99% certain that \mathcal{N} lies between 351.62 and 358.86. The red region in **Figure 3** shows how the credible interval for \mathcal{N} depends on the probability that the truth lies within that interval.

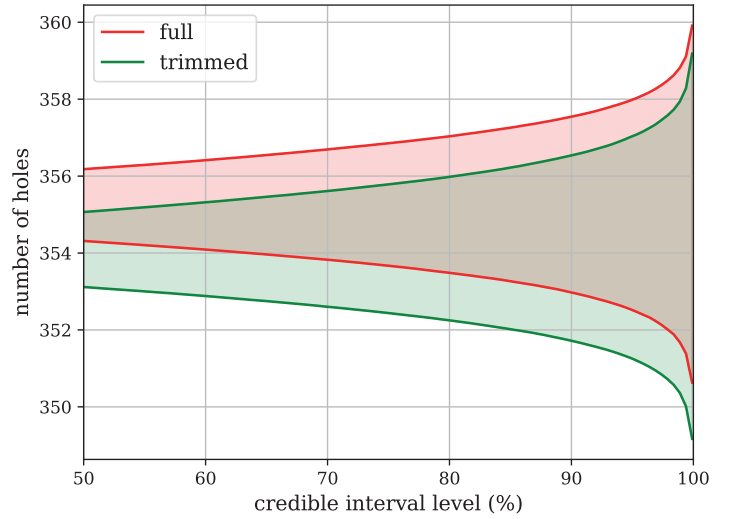


Figure 3. The range of values for the number of holes in the full calendar ring, as a function of the probability that the interval contains the true value. The result from the full set of holes in section 1, 2, 3, 5, 6 and 7 are in red, and those from the trimmed dataset (section 1, 2, 3 and 7, excluding leading and trailing holes) in green.

3.3. Integer Values for the Number of Holes

Up to this point we have taken \mathcal{N} to be a continuous parameter, allowing for a single spacing discontinuity between holes in a lost section of the ring, or indeed that the original ring was not fully populated with holes. However, it is reasonable to consider that there was no such discontinuity in the original ring, and that \mathcal{N} is an integer. This is equivalent to setting a prior for \mathcal{N} that consists of a series of delta functions at discrete integer values.

As we initially used a uniform prior for \mathcal{N} , this new prior can be applied to the posterior post-marginalisation. However, rather few samples will land close to these integer points, so it is useful to take values from a continuous estimate for the probability density. **Figure 4A** indicates that the posterior for \mathcal{N} is a very close to Gaussian, so we use a Gaussian as this continuous function,

$$p(\mathcal{N} | \{\mathbf{d}_{ij}\}) = \frac{1}{(2\pi)^{1/2} \sigma_{\mathcal{N}}} \exp\left[-\frac{(\mathcal{N} - \bar{\mathcal{N}})^2}{2\sigma_{\mathcal{N}}^2}\right], \quad (10)$$

characterised by the marginal posterior mean $\bar{\mathcal{N}} = 355.249$, and standard deviation $\sigma_{\mathcal{N}} = 1.390$ of the MCMC chain. We can now compute probabilities for \mathcal{N} from this function evaluated at the discrete values singled-out by the prior. These normalised probabilities, based on all the data, are shown in the centre column of **Table 2**, and are shown graphically in the blue plot of **Figure 4B**.

As a cross-check, we used the nested sampling analysis to compare the relative probabilities of a set of models that assumed integer values for \mathcal{N} . Again, these produced results that were consistent with Gaussian approximation presented here.

N	Prob (N all)	Prob (N trim)
349	0.0000	0.0006
350	0.0002	0.0055
351	0.0027	0.0293
352	0.0187	0.0978
353	0.0776	0.2056
354	0.1917	0.2714
355	0.2823	0.2251
356	0.2479	0.1173
357	0.1298	0.0384
358	0.0405	0.0079
359	0.0075	0.0010
360	0.0008	0.0001
361	0.0001	0.0000

Table 2. The probabilities that the full calendar ring contained N equally spaced holes, given the full dataset (column 2), the trimmed dataset (column 3) and our model assumptions.

3.4. A Trimmed Dataset

The preceding analysis has implicitly assumed that the section divisions identify all the discontinuities in the ring fragment. However, Budiselic *et al.* highlight the difficulty in identifying all of these unambiguously from the X-ray images, and there may be further discontinuities in hole placement that are not listed. Given the sections are defined by the locations of cracks, we can consider whether the first and last holes of each section are as trustworthy as the rest, as they are by definition adjacent to damage.

Let us therefore consider a reduced, and possibly safer, dataset. We will exclude the short segments (S5, S6) entirely, and the first and last holes of the remaining sections S1, S2, S3 and S7 (that is, we exclude holes 2, 23, 24, 32, 33, 69, 76 and 81). The sections are now shorter and fewer, so we would expect the uncertainties in our derived model parameters to grow slightly. However, in return, we are somewhat more confident that the data comprises the evenly spaced holes affected by statistically stationary errors assumed by the model.

Table 3 shows the intrinsic parameters derived using this reduced dataset. The differences are relatively minor, but the values of r and N are slightly reduced. Although these results are based on fewer holes, they are probably slightly more robust than the full dataset solutions. The corresponding probabilities of integer N values are shown in the third column of Table 2, and the orange bars in the plot of Figure 4B.

4. Conclusions

Budiselic *et al.* made careful and precise measurements of hole positions beneath the Antikythera calendar ring, and identified displaced sections of the fragment. We combined these measurements with a simple model of how they differ from ideal values on a circle. This was based on a Gaussian distribution that distinguished between the magnitude of error displacements tangential and perpendicular to the circle. We used this to form a joint likelihood function for the radius of the full circle, the number of holes it contained and the displacement parameters of the broken sections.

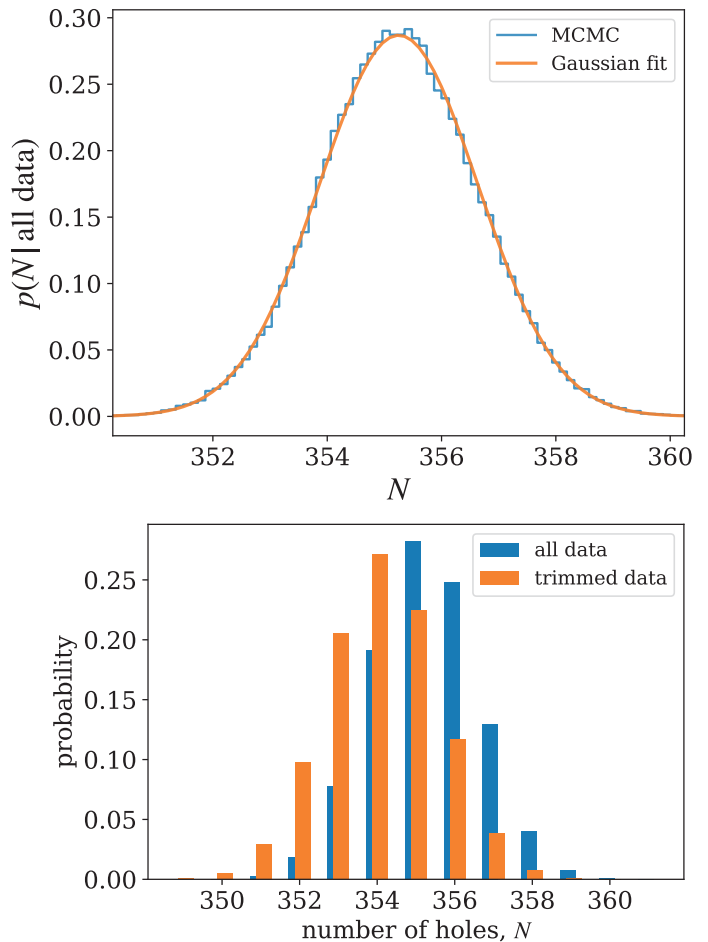


Figure 4A, Top: the Gaussian fit to the marginal posterior for N , given the full dataset. Figure 4B, Bottom: the data from Table 2, based on Gaussian, fits to the full and trimmed datasets, displayed graphically.

Parameter	Median	68%	90%	95%	99%
r	77.11	+0.30 -0.29	+0.50 -0.48	+0.60 -0.57	+0.81 -0.77
N	354.08	+1.47 -1.41	+2.46 -2.36	+2.96 -2.83	+3.92 -3.77
σ_r	0.026	+0.003 -0.002	+0.005 -0.004	+0.006 -0.004	+0.008 -0.005
σ_t	0.122	+0.012 -0.010	+0.021 -0.016	+0.025 -0.019	+0.035 -0.024

Table 3. The intrinsic parameters of the calendar ring holes, derived from the reduced dataset. Again, lengths are in millimetres.

After combining this likelihood with uninformative priors, we computed the joint and marginal posterior probability distributions of these parameters using stochastic sampling methods, which we marginalised to determine the probability distribution for the number of holes.

Budiselic *et al.*'s paper addressed whether the calendar ring holes represented the 365 days of the Egyptian civil calendar or the 354 days of the lunar calendar. We agree with these authors that the number of holes beneath the ring is consistent with 354 days, but not with 365. Additionally, our statement on the number of holes is significantly more constraining.

Using all the data, the 354-hole hypothesis is about 229 times more probable than 360 holes, which they also considered, and vastly more probable than 365 holes.

However, we have not been able to definitively constrain \mathcal{N} to a particular integer, or indeed show that it is an integer.

If we remove holes at the extremities of the sections, that might be affected by fracture, the 68%-credible bound on \mathcal{N} becomes $354.08^{+1.47}_{-1.41}$.

A deeper analysis of the dataset is, of course, possible. One could relax the coplanar assumption and introduce a small z displacement to each section, and include the remaining two Euler angles for each section's orientation out of the plane. This would add another 18 parameters to the model.

Additionally, one could use Bayesian methods to infer the number and positions of segment divisions, rather than rely on the choices made by Budiselic *et al.* These additional degrees of freedom would inevitably increase the uncertainty in the intrinsic parameters. We note, however, that the need for these additional degrees of freedom would be revealed by systematic discrepancies between the posterior predictive point-clouds and the measured hole positions, shown in **Figure 1**. Given there is no such clear discrepancy, we can assume that the current model has captured the essence of the problem, and that it is unlikely the conclusions would be significantly affected by including them.

REFERENCES

1. Chris Budiselic *et al.*, 'Antikythera Mechanism Shows Evidence of Lunar Calendar', *Horological Journal*, vol. 163 (March 2021), pp104–112; doi: 10.7910/DVN/VJGLVS. SocArXiv: fzp8u. <<https://bhi.co.uk/wp-content/uploads/2020/12/BHI-Antikythera-Mechanism-Evidence-of-a-Lunar-Calendar.pdf>> last accessed 22 May 2024.
2. Daniel Foreman-Mackey *et al.*, 'emcee: The MCMC Hammer', *Publications of the Astronomical Society of the Pacific* 125.925 (March 2013), p306; doi: 10.1086/670067. arXiv: 1202.3665 [astro-ph.IM].
3. Seiradakis, J. H., Edmunds, M. G., 'Our current knowledge of the Antikythera Mechanism', *Nature Astronomy* 2 (Jan 2018), pp35–42; doi: 10.1038/s41550-017-0347-2.
4. Joshua S. Speagle, 'dynesty: a dynamic nested sampling package for estimating Bayesian posteriors and evidences', *Monthly Notices of the Royal Astronomical Society* 493.3 (Feb 2020), pp3132–3158; issn: 0035-8711; doi: 10.1093/mnras/staa278. E-print <<https://academic.oup.com/mnras/article-pdf/493/3/3132/32890730/staa278.pdf>> last accessed 22 May 2024; <<https://doi.org/10.1093/mnras/staa278>> last accessed 22 May 2024.
5. Andrew Thoeni, Chris Budiselic, Andrew Ramsey, 'Replication Data for: Antikythera Mechanism Shows Evidence of Lunar Calendar', version V3, *Harvard Dataverse* (2019); doi: 10.7910/DVN/VJGLVS. <<https://doi.org/10.7910/DVN/VJGLVS>> last accessed 22 May 2024.

Graham Woan

Graham Woan is Professor of Astrophysics and Observatory Director at the University of Glasgow. He began his career in radio astronomy, working in long baseline interferometry and later in interplanetary weather. Since 2000 he has been a member of the LIGO Scientific Collaboration, concentrating on the search for gravitational waves from spinning neutron stars. He is part of the team developing data analysis methods for the Laser Interferometer Space Antenna (LISA), recently adopted by the European Space Agency (ESA), and due for launch around 2035.



Joseph Bayley

Joseph Bayley is a Research Associate at the University of Glasgow primarily working in gravitational wave data analysis. He completed his PhD at the University of Glasgow in 2020 focusing on searching for rapidly rotating neutron stars in gravitational wave data. He is a member of the LIGO Scientific Collaboration where he continues to run searches for neutron stars and focuses on how machine learning can be used to improve data analysis within various parts of gravitational wave astronomy and instrumentation.



HJ's policy is to operate a double-blind peer-review. This independent rigour ensures the validity and accuracy of what is published. This paper by Woan & Bayley was deposited with arXiv, an online pre-print server, on 29 February 2024. It has become the practice in academia to submit papers to online resources such as arXiv before they are peer-reviewed. The paper was then submitted to *HJ* on 6 March 2024, and cleared by the peer-reviewer (a professor overseas) on 22 April. The related paper, 'How Many Days in an Egyptian Year' by Dickens & Malin (*HJ*, April 2024) had been peer-reviewed by 21 February, and cleared for printing on 26 February 2024; by 22 April it was already on the presses.